Improvements and limitations of Mie n-6 potential for condensed phase viscosity prediction at saturation and elevated pressures

Richard A. Messerly

Thermodynamics Research Center, National Institute of Standards and Technology, Boulder, Colorado, 80305

Michelle C. Anderson

Thermodynamics Research Center, National Institute of Standards and Technology, Boulder, Colorado, 80305

S. Mostafa Razavi

Department of Chemical and Biomolecular Engineering, The University of Akron

J. Richard Elliott

Department of Chemical and Biomolecular Engineering, The University of Akron

Abstract

While many common force fields are developed based on liquid density and heat of vaporization at room temperature, several more recent force fields have taken into account saturated vapor pressure and saturated liquid density over substantial portions of the vapor-liquid coexistence curve for multiple compounds simultaneously, enhancing transferability. This manuscript explores the hypothesis that greater accuracy in characterizing the coexistence properties may lead to greater accuracy for viscosity predictions. Four united atom force fields are considered in detail: the TraPPE-UA model of Siepmann and coworkers, the TAMie model of Gross and coworkers, the AUA4 model of Ungerer and coworkers, and the TraMie model of Potoff and coworkers. Equilibrium molecular dynamics simulations are performed in the NVT ensemble using the Green-Kubo method for viscosity characterization. Simulations are performed for linear alkanes with two to sixteen carbons and branched

alkanes with four to nine carbons. Simulation conditions follow the saturated liquid from reduced temperatures of 0.5 to 0.9 and along the 293 K isotherm in the dense liquid region.

In general, the more accurate force fields for coexistence properties do indeed predict viscosity more accurately. For saturated liquids, both the TraMie and TAMie models provide roughly 10 % accuracy for linear alkanes, while deviations are closer to 20 to 50 % for AUA4 and TraPPE-UA models. For branched alkanes, the behavior is more complicated but TraMie still provides roughly 15 to 20 % accuracy, while the TAMie force field results in deviations of 20 to 40 %, and the TraPPE-UA and AUA4 force fields have deviations of approximately 25 to 60 %. The deviations tend to increase with decreasing temperature, with the exception of the TraMie deviations for propane, which are nearly constant to the triple point temperature.

For compressed liquids, the Mie potential models perform better once again, but tend to overestimate the viscosity at very high densities. Coincidentally, these models also tend to overestimate the pressure at high densities, such that plots of viscosity with respect to pressure are accurate to within about 10 % up to 200 MPa. Experimental viscosity data tend to be sparse above 200 MPa, but accurate predictions are obtained for propane to 1 GPa. Uncertainty estimates increase substantially for high pressures at low reduced temperatures. Nevertheless, a prediction is made for the viscosity of 2,2,4-trimethylpentane at 293K and 1 GPa.

---

1. Introduction

The design of efficient and reliable technical processes requires accurate estimates of thermophysical properties. Shear viscosity (η) is an important property for characterizing flow, e.g., sizing pumps, assessing flow assurance in fossil fuel recovery, and lubricating bearings in tribological applications. There are primarily three different means by which shear viscosity estimates are obtained: experimental measurement, semi-empirical prediction models, and molecular simulation (molecular dynamics, MD). Significant limitations exist for each of these methods.

For example, experimental measurements can be expensive, time-consuming, and challenging at extreme temperatures (T) and pressures (P). Experimental data tend to be distributed among several prototypes of linear, branched, ring, and polar molecules, with many gaps among a homologous series. Most experimental data are available below 200 MPa, while tribological applications may require estimates at pressures as high as 1 GPa. Flow assurance applications are generally at pressures below 200 MPa, but at temperatures of 423 to 523 K. These ever expanding conditions of interest and economic constraints on new measurements foster increased research in predictive methods.

The National Institute of Standards and Technology (NIST) Reference Fluid Properties (REFPROP) provides "reference quality" viscosity correlations for experimentally well-studied compounds (around 100 species). Most compounds do not have sufficient *reliable* experimental data covering a wide range of temperatures, pressures, and densities (ρ) for developing "reference quality" correlations. These compounds require predictive methods that pool together data from several related molecular species.

Semi-empirical prediction models are typically not reliable over the industrially relevant ranges of $P\rho T$ [1]. For example, corresponding states methods are recommended for vapors, dense fluids, and high temperature liquids [?]. These methods rely on the similarity of trends in the properties relative to a reference compound, e.g., methane and *n*-octane. Corresponding states methods are less reliable for more complex molecular structures, e.g., branched compounds. Typical compilations indicate that deviations from experiment may vary by 5 to 50 %, with little guidance about when to expect lower or higher accuracy. For low temperature liquids, group contribution schemes are favored, but these tend to extrapolate poorly when applied to compounds or conditions outside the training set. More recent advances such as machine learning [2, 3] and entropy scaling [4] have shown great promise. However, machine learning relies on large amounts of experimental data and extrapolates poorly due to its weak theoretical basis. While entropy scaling has a stronger theoretical basis, it requires a reliable reference viscosity and an adequate equation-of-state, which may not be readily available for the compound of interest.

There are two fundamental challenges for utilizing molecular simulation to estimate viscosity. First, obtaining reproducible results is more difficult for transport properties, such as viscosity, than for static properties. Second, viscosity is extremely sensitive to the force field. In addition to the strong dependence on the non-bonded interactions, the bonded potential plays a much greater role for viscosity than for static properties. For example, varying the torsional potential has a significant impact on viscosity, [5] while vapor-liquid coexistence is relatively unaffected [6]. Therefore, the ability to predict viscosities with molecular simulation requires both robust methods and adequate force fields.

Recently, a "Best Practices Guide" was developed to address the first challenge, namely, to improve reproducibility [7]. We apply the "Best Practices" and address some outstanding issues mentioned therein. However, the focus of this study is the second challenge, namely, determining the most accurate force field(s). We investigate the accuracy of united-atom (UA) Mie n-6 force fields, a popular class designed for the engineering purpose of predicting thermophysical properties. Specifically, the force fields we compare are the Transferable Potential for Phase Equilibria TraPPE-UA (and TraPPE-UA2), Transferable Anisotropic Mie (TAMie), Potoff, and fourth generation anisotropic-united-atom (AUA4). Recently, it was shown that the Mie 14-6 and 16-6 potentials of TAMie and Potoff, respectively, are overly repulsive at high densities/pressures. The suitability of these force fields for quantitative viscosity prediction has been widely debated in the literature.

For example, some studies suggest that, depending on the compound structure and state conditions, united-atom models are inadequate for estimating viscosities and recommend the use of anisotropic-united-atom (AUA) or all-atom (AA) models for this purpose [8, 9, 10, 11]. However, these studies focused primarily on UA Lennard-Jones (LJ) 12-6 force fields. Reference 12 provides evidence that the UA Mie n-6 potential can accurately predict saturated liquid viscosity ($\eta_{\mathrm{liq}}^{\mathrm{sat}}$) without significant deprecation of other vapor-liquid saturation properties, i.e., saturated liquid density ($\rho_{\mathrm{liq}}^{\mathrm{sat}}$), saturated vapor density ($\rho_{\mathrm{vap}}^{\mathrm{sat}}$), and saturated vapor pressure ($P_{\mathrm{vap}}^{\mathrm{sat}}$). Alternatively, Reference 5 demonstrated significant improvement in viscosity prediction by modifying the AUA4 torsional potential (AUA4m). Considering the signifi-

cant increase in computational cost of AA simulations, Mie n-6 and/or modified torsional potentials are a desirable alternative to AA force fields.

The force fields compared in this study were optimized solely with vapor-liquid coexistence data, i.e., dynamic properties, such as viscosity, were not included in their parameterization. While the Potoff and TAMie force fields have shown considerable promise in predicting static properties (primarily $P_{\text{vap}}^{\text{sat}}$), their ability to predict dynamic properties has not been investigated previously. Reference 13 demonstrates that including viscosity data in the force field development can improve the identification of a unique set of transferable Mie n-6 parameters, while improving viscosity predictions simultaneously. Notwithstanding the potential benefits of including viscosity as a property of interest during force field development, we assess the accuracy of TraPPE-UA, TAMie, Potoff, and AUA4 for estimating viscosity as they currently stand, including their torsional potential models.

The outline for the present work is the following. Section 2 explains the force fields, simulation methodology, and data analysis. Section 3 presents the simulation results for each force field, compound, and state point studied. Section 4 discusses some important observations and limitations. Section 5 recaps the primary conclusions from this work.

2. Methods

2.1. Force field

A united-atom (UA) or anisotropic-united-atom (AUA) representation is used for each compound studied, i.e., normal and branched alkanes are represented with CH_3, CH_2, CH, and C sites. UA models assume that the UA interaction site is that of the carbon atom, while AUA models assume that the AUA interaction site is shifted away from the carbon atom and towards the hydrogen atom(s). Note that TraPPE and Potoff are UA force fields while TraPPE-2, AUA4, and TAMie are AUA force fields.

The results presented in this work utilize fixed bond-lengths, where each bond not involving a CH_3 site utilizes a 0.154 nm bond-length. The anisotropic-united-atom models (TAMie, AUA4, and TraPPE-2) use a slightly larger "effective" bond-length for CH_3 bonds

(see Table 1). While the TAMie force field modifies only the terminal CH_3 sites, AUA4 displaces the interaction location of CH_2 and CH sites as well. For simplicity, we only utilize the AUA4 force field with compounds that are composed exclusively of CH_3 and C interaction sites, i.e., ethane and 2,2-dimethylpropane.

Table 1: Effective bond-lengths in units of nm for terminal (CH_3) UA or AUA interaction sites. Empty table entries for TraPPE-2 denote that the force field does not contain the corresponding interaction site type. Empty table entries in AUA4 arise because this force field uses a more complicated construction than the simple effective bond-length approach. Specifically, AUA4 requires CH_2 and CH interaction sites that are not along the C-C bond axis.

Bond	TraPPE, Potoff	TAMie	AUA4	TraPPE-2
CH_3-CH_3	0.154	0.194	0.1967	0.230
CH_3-CH_2	0.154	0.174	–	–
CH_3-CH	0.154	0.174	–	–
CH_3-C	0.154	0.174	0.1751	–

Although static thermodynamic properties (e.g., $\rho_{\text{liq}}^{\text{sat}}$) are generally insensitive to the choice of fixed or flexible bonds, dynamic properties (e.g., η) are much more sensitive. For this reason, we test the degree of variability that arises by implementing a harmonic oscillator model. The results are provided as Supporting Information.

The same angle and dihedral potentials are used for each force field. Angular bending interactions are evaluated using a harmonic potential:

$$u^{\text{bend}} = \frac{k_\theta}{2} \left(\theta - \theta_0 \right)^2 \tag{1}$$

where u^{bend} is the bending energy, θ is the instantaneous bond angle, θ_0 is the equilibrium bond angle (see Table 2), and k_θ is the harmonic force constant which is equal to 62500 K/rad^2 for all bonding angles. Dihedral torsional interactions are determined using a cosine series:

$$u^{\text{tors}} = c_0 + c_1[1 + \cos \phi] + c_2[1 - \cos 2\phi] + c_3[1 + \cos 3\phi] \tag{2}$$

6

where u^{tors} is the torsional energy, ϕ is the dihedral angle and c_i are the Fourier constants listed in Table 3.

Table 2: Equilibrium bond angles (θ_0). x and y are values between 0 and 3.

Bending sites	θ_0 (degrees)
CH_x-CH_2-CH_y	114.0
CH_x-CH-CH_y	112.0
CH_x-C-CH_y	109.5

Table 3: Fourier constants (c_i) in units of K. x and y are values between 0 and 3.

Torsion sites	c_0	c_1	c_2	c_3
CH_x-CH_2-CH_2-CH_y	0.0	355.03	-68.19	791.32
CH_x-CH_2-CH-CH_y	-251.06	428.73	-111.85	441.27
CH_x-CH_2-C-CH_y	0.0	0.0	0.0	461.29
CH_x-CH-CH-CH_y	-251.06	428.73	-111.85	441.27

Non-bonded interaction energies and forces between sites located in two different molecules or separated by more than three bonds within the same molecule are calculated using a Mie n-6 potential (of which the Lennard-Jones, LJ, 12-6 is a subclass) [14]:

$$u^{\text{vdw}}(\epsilon, \sigma, n; r) = \left(\frac{n}{n-6}\right)\left(\frac{n}{6}\right)^{\frac{6}{n-6}} \epsilon \left[\left(\frac{\sigma}{r}\right)^n - \left(\frac{\sigma}{r}\right)^6\right] \tag{3}$$

where u^{vdw} is the van der Waals interaction, σ is the distance (r) where $u^{\text{vdw}} = 0$, $-\epsilon$ is the energy of the potential at the minimum $\left(\text{i.e., } u^{\text{vdw}} = -\epsilon \text{ and } \frac{\partial u^{\text{vdw}}}{\partial r} = 0 \text{ for } r = r_{\min}\right)$, and n is the repulsive exponent. The non-bonded Mie n-6 force field parameters for TraPPE, TraPPE-2, Potoff, AUA4, and TAMie are provided in Table 4.

Note that TraPPE (TraPPE-2) and TAMie implement an ethane-specific set of CH_3 parameters. Also, Potoff reports a "generalized" and "short/long" (S/L) CH and C parameter

Table 4: Non-bonded (intermolecular) parameters for TraPPE [15, 16] (and TraPPE-2 [17]), Potoff [18, 19], AUA4 [20, 21], and TAMie [22, 23] force fields. The "short/long" Potoff CH and C parameters are included in parentheses. The ethane specific parameters for TAMie are included in parentheses.

United-atom	TraPPE (TraPPE-2)			Potoff (S/L)		
	ϵ (K)	σ (nm)	n	ϵ (K)	σ (nm)	n
CH_3	98 (134.5)	0.375 (0.352)	12	121.25	0.3783	16
CH_2	46	0.395	12	61	0.399	16
CH	10	0.468	12	15 (15/14)	0.46 (0.47/0.47)	16
C	0.5	0.640	12	1.2 (1.45/1.2)	0.61 (0.61/0.62)	16
	AUA4			TAMie		
CH_3	120.15	0.3607	12	136.318 (130.780)	0.36034 (0.36463)	14
CH_2	86.29	0.3461	12	52.9133	0.40400	14
CH	50.98	0.3363	12	14.5392	0.43656	14
C	15.04	0.244	12	–	–	–

set. The "short" and "long" parameters are implemented when the number of carbons in the backbone is ≤ 4 and > 4, respectively. Due to their improved performance, we only provide results for the Potoff S/L parameter set.

Non-bonded interactions between two different site types (i.e. cross-interactions) are determined using Lorentz-Berthelot combining rules [24] for ϵ and σ, respectively, and an arithmetic mean for the repulsive exponent n (as recommended in Reference 18):

$$\epsilon_{ij} = \sqrt{\epsilon_{ii}\epsilon_{jj}} \tag{4}$$

$$\sigma_{ij} = \frac{\sigma_{ii} + \sigma_{jj}}{2} \tag{5}$$

$$n_{ij} = \frac{n_{ii} + n_{jj}}{2} \tag{6}$$

where the ij subscript refers to cross-interactions and the subscripts ii and jj refer to same-site interactions.

2.2. Simulation set-up

Viscosity estimates can be obtained from both equilibrium molecular dynamics (EMD) and non-equilibrium molecular dynamics (NEMD) simulations. The "Best Practices Guide" is currently limited to EMD methods and purports that NEMD might be necessary for high viscosities (greater than 0.02 Pa-s). One purpose of the present work is to demonstrate that, by applying these guidelines, EMD can also provide meaningful estimates for highly viscous systems.

Equilibrium molecular dynamics simulations are performed using GROMACS version 2018 [25]. GROMACS was compiled using the BLANK compiler and run on a BLANK. Example GROMACS input files (.top, .gro. and .mdp) are provided as Supporting Information. In addition, the shell and python scripts used for preparing and analyzing simulations are available on GitHub [?]. The simulation specifications are provided in Tables 5 and 6.

Table 5: General simulation specifications.

Time-step (fs)	2
Equilibration time (ns)	1
Production time (ns)	1, 2, 4, or 8
Cut-off length (nm)	1.4 (1.0 for Potoff)
Tail-corrections [26]	U and P
Constrained bonds	LINCS
LINCS-order	8
Number of molecules	400

Note that the non-bonded cut-off distance is 1.4 nm for each force field except Potoff, which employs a 1.0 nm cut-off (as recommended by the authors). For most systems, 1 ns is a sufficient production time, while longer simulations are required for the more viscous systems, e.g., 2,2,4-trimethylpentane at elevated pressures.

Following "Best Practices", we compute η with several different production times (1, 2, 4,

Table 6: Integrator, thermostat and barostat specifications.

	NPT Equil.	NPT Prod.	NVT Equil.	NVT Prod.
Integrator	Velocity Verlet	Leap frog	Velocity Verlet	Velocity Verlet
Thermostat	Velocity rescale	Nosé-Hoover	Nosé-Hoover	Nosé-Hoover
Thermostat time-constant (ps)	1.0	1.0	1.0	1.0
Barostat	Berendsen	Parrinello-Rahman	N/A	N/A
Barostat time-constant (ps)	1.0	5.0	N/A	N/A
Barostat compressibility	4.5e-5	4.5e-5	N/A	N/A

and 8 ns) for select systems to verify that the results are indistinguishable (see Supporting Information). Furthermore, we investigate system size effects by comparing results with 100, 200, 400, and 800 molecules (see Section 4). In addition, we compare fixed and flexible bonds in the Supporting Information.

When the viscosity is desired at a prescribed temperature and density ($\eta(\rho,T)$), three stages are required: energy minimization, NVT equilibration, and NVT production. When the viscosity is desired at a prescribed temperature and pressure ($\eta(P,T)$), five stages are required: energy minimization, NPT equilibration, NPT production, NVT equilibration, and NVT production. Note that, according to "Best Practices", the final production stage simulations are always performed using the NVT ensemble.

As recommended by "Best Practices," we utilize 30 to 60 independent replicates to improve the precision and to provide more rigorous estimates of uncertainty. To ensure independence between replicates, the entire series of MD simulations are repeated for each replicate.

Two different classes of viscosity are investigated in this study, namely, saturated liquid viscosity ($\eta_{\text{liq}}^{\text{sat}}$) and compressed liquid viscosities at a temperature of 293 K ($\eta_{\text{liq}}^{\text{comp}}$). Saturated liquid viscosities are estimated by performing NVT ensemble simulations at the saturation

temperature (T^{sat}) and saturated liquid density ($\rho_{\text{liq}}^{\text{sat}}$). The simulation densities correspond to the REFPROP $\rho_{\text{liq}}^{\text{sat}}$, which is admittedly not necessarily the same as the force field $\rho_{\text{liq}}^{\text{sat}}$. This point is discussed in greater detail in Section 4.

Two different simulation protocols are implemented for estimating compressed liquid viscosities ($\eta_{\text{liq}}^{\text{comp}}$). Specifically, we perform simulations with each force field either at the same ρ or the same P. For the purpose of comparing trends between force fields and REFPROP, these two methods are essentially equivalent. From a practical standpoint, estimating η at a given P requires performing preliminary NPT ensemble simulations to determine the corresponding box size.

2.3. Data analysis

Following the "Best Practices" recommendation, we implement the Green-Kubo "time-decomposition" analysis to extract viscosity from EMD simulations. We refer the interested reader to References 7 and 27 for further details. In brief, the Green-Kubo integral is computed with respect to time according to

$$\eta(t) = \frac{V}{3k_{\text{B}}TN_{\text{reps}}} \sum_{n=1}^{N_{\text{reps}}} \sum_{\alpha \neq \beta} \int_0^t dt' \left\langle \tau_{\alpha\beta,n}(t')\tau_{\alpha\beta,n}(0) \right\rangle_{t_0} \tag{7}$$

where V is the volume, k_{B} is the Boltzmann constant, $\langle \cdots \rangle_{t_0}$ denotes an average over time origins, α and $\beta = x, y$, or z Cartesian coordinates, and $\tau_{\alpha\beta,n}$ is the α-β off-diagonal stress tensor element for the nth replicate.

$\tau_{\alpha\beta,n}$ is recorded every 6 fs (3 time-steps) to adequately integrate the initial rapid decay of the autocorrelation function. To improve precision, Equation 7 averages several (between 30 and 60) independent replicate simulations (N_{reps}), twelve different time-origins (t_0), and all three unique off-diagonal components of τ (hence the factor of 3 in the denominator of Equation 7).

The "true" viscosity is obtained by evaluating Equation 7 in the infinite-time-limit, i.e., as $t \rightarrow \infty$. However, the long-time tail of the Green-Kubo integral is often quite noisy and does not converge nicely. For this purpose, we fit a double-exponential function to the "running

11

integral"

$$\eta(t) = A\alpha\tau_1 \left(1 - \exp\left(-t/\tau_1\right)\right) + A(1 - \alpha)\tau_2 \left(1 - \exp\left(-t/\tau_2\right)\right) \tag{8}$$

where A, α, τ_1, and τ_2 are fitting parameters and $\eta^{\infty} = A\alpha\tau_1 + A(1 - \alpha)\tau_2$ is the infinite-time-limit viscosity.

Since the Green-Kubo "running integral" suffers from extreme fluctuations at long times, Equation 8 is fit by minimizing a weighted sum-squared error objective function. Weights are equal to the inverse of the standard deviation (σ_η) of the replicate simulations. The dime dependence of σ_η is modeled with At^b, where A and b are fitting parameters.

Following a heuristic proposed in Reference 27, data are excluded where $\sigma_\eta > 0.4 \times \eta^{\infty}$. Occasionally this heuristic resulted in a cut-off that was too short, which lead to very poor fits. In such cases, it was necessary to modify the heuristic to $0.8 \times \eta^{\infty}$.

Erroneously large fluctuations also exist at very short times. Following "Best Practices," only data for $t > 3$ ps are included in the fitting of Equation 8.

As recommend by "Best Practices", uncertainties are obtained by bootstrap re-sampling. Specifically, the fitting process described previously is repeated hundreds of times using randomly selected subsets of replicate simulations. Furthermore, each repetition uses a randomly selected long-time cut-off to account for the uncertainty in the % heuristic. A 95 % confidence interval is obtained from the distribution of bootstrap estimates for η^{∞}. An example of this process is provided as Supporting Information.

3. Results

Seven normal and seven branched alkanes of varying chain-length and degree of branching are simulated in this study. We only consider compounds with available REFPROP equations-of-state and viscosity correlations [28]. Specifically, we simulate ethane [29, 30], propane [31, 32], n-butane [33, 34], n-octane [35, 36], n-dodecane [37, 38], n-hexadecane [39, 40], n-docosane [39, 41], 2-methylpropane [42, 43], 2-methylbutane [42, 41], 2-methylpentane [42, 41], 3-methylpentane [44, 41], 2,2-dimethylpropane [42, 41], 2,3-dimethylbutane [44, 41], and 2,2,4-trimethylpentane [45, 41].

Each compound was simulated using the TraPPE (UA LJ 12-6) and Potoff S/L (UA Mie 16-6) force fields. Potoff "short" parameters are used for 2-methylpropane, 2-methylbutane, 2,2-dimethylpropane, and 2,3-dimethylbutane while Potoff "long" parameters are utilized for 2-methylpentane, 3-methylpentane, and 2,2,4-trimethylpentane. 2,2-dimethylpropane and 2,2,4-trimethylpentane were not simulated using the TAMie (AUA Mie 14-6) force field since we are not aware of any TAMie parameters for C sites. Only ethane and 2,2-dimethylpropane were simulated with AUA4 (AUA LJ 12-6).

Table 7 demonstrates which compounds, force fields, and viscosity types were simulated in this study.

Table 7: Compounds, force fields, and state points. "X": simulated, "O": not simulated, "S" simulated with "Short" parameters, "L" simulated with "Long" parameters.

Compound	TraPPE (TraPPE-2)		Potoff (S/L)		AUA4		TAMie	
	$\eta_{\mathrm{liq}}^{\mathrm{sat}}$	$\eta_{\mathrm{liq}}^{\mathrm{comp}}$	$\eta_{\mathrm{liq}}^{\mathrm{sat}}$	$\eta_{\mathrm{liq}}^{\mathrm{comp}}$	$\eta_{\mathrm{liq}}^{\mathrm{sat}}$	$\eta_{\mathrm{liq}}^{\mathrm{comp}}$	$\eta_{\mathrm{liq}}^{\mathrm{sat}}$	$\eta_{\mathrm{liq}}^{\mathrm{comp}}$
ethane	X	X	X	X	X	X	X	X
propane	X	X	X	X	O	O	X	X
n-butane	X	X	X	X	O	O	X	X
n-octane	X	X	X	X	O	O	X	X
n-dodecane	X	O	X	O	O	O	X	O
n-hexadecane	X	O	X	O	O	O	X	O
2-methylpropane	X	X	S	S	O	O	X	X
2-methylbutane	X	X	S	S	O	O	X	X
2,2-dimethylpropane	X	X	S	S	X	X	O	O
2,3-dimethylbutane	X	X	S	S	O	O	X	X
2-methylpentane	X	X	L	L	O	O	X	X
3-methylpentane	X	X	L	L	O	O	X	X
2,2,4-trimethylpentane	X	X	L	L	O	O	O	O

Sections 3.1 and 3.2 present results for saturated liquid viscosities and compressed liquid viscosities, respectively. In both sections, the *n*-alkane results are followed by the branched alkane results. Simulation results are compared with the REFPROP viscosity correlations and experimental data from the ThermoData Engine (TDE) database [46].

3.1. Saturated Liquid

3.1.1. Normal alkanes

Figure 1 compares the TraPPE (UA LJ 12-6), TraPPE-2 (AUA LJ 12-6), TAMie (AUA Mie 14-6), Potoff (UA Mie 16-6), and the Bayesian parameter sets for $n = 13$, 14, 15, and 16.
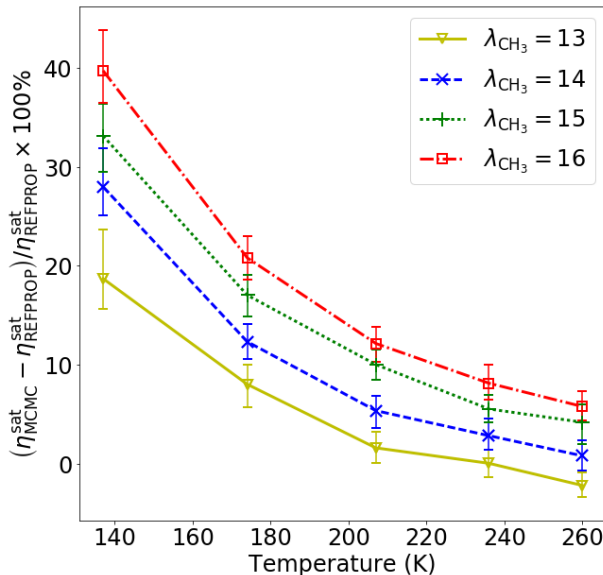
Figure 1: Saturated liquid viscosities for ethane. Colors/symbols denote different force fields.

Figure 2 compares the TraPPE (UA LJ 12-6), Potoff (UA Mie 16-6), and TAMie (AUA Mie 14-6) saturated liquid viscosities for propane, *n*-butane, and *n*-octane. Similar to what has been demonstrated in previous studies, the TraPPE force field significantly under predicts $\eta_{\text{liq}}^{\text{sat}}$ (between 30 and 80 %) with the deviation increasing with decreasing temperature. By contrast, the Potoff and TAMie force fields agree with the REFPROP values for these compounds to within 10 %. While TAMie deviations increase near the triple point temper-

ature of propane, Potoff deviations are nearly constant over the entire temperature range studied for each compound.
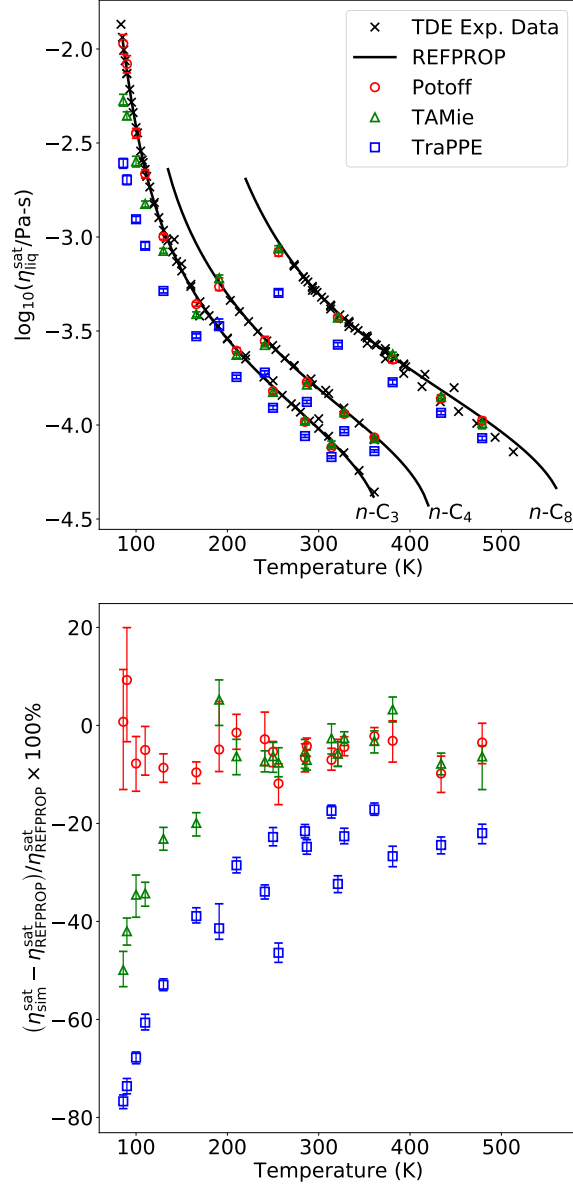

Figure 2: Saturated liquid viscosities for propane (n-C$_3$), n-butane (n-C$_4$), and n-octane (n-C$_8$). Top panel compares simulation results with REFPROP correlations and TDE data. Bottom panel computes the percent deviation between the simulation and REFPROP values. Colors/symbols denote different force fields.

Figure 3 compares the TraPPE, Potoff, and TAMie saturated liquid viscosities for n-

dodecane, n-hexadecane, and n-docosane. Although the TraPPE results for these compounds are similar to those observed in Figure 2 for smaller n-alkanes, TAMie and Potoff demonstrate a stronger temperature dependence for these larger n-alkanes. The cause of this trend is unclear but, since it is only observed for larger compounds, it is likely attributed to the torsional potential or the transferability of the CH$_2$ Mie n-6 parameters.

3.1.2. Branched alkanes

Figures 4 and 5 compare the saturated liquid viscosities for each force field and branched alkane studied. Figures 4 and 5 present results for the compounds classified by Potoff as "short" and "long", respectively. Specifically, Figure 4 depicts 2-methylpropane, 2,2-dimethylpropane, 2-methylbutane, and 2,3-dimethylbutane, while Figure 5 contains 2-methylpentane, 3-methylpentane, and 2,2,4-trimethylpentane. Each compound was simulated using the TraPPE (UA LJ 12-6) and Potoff (UA Mie 16-6) force fields. However, only 2,2-dimethylpropane was simulated with AUA4 (AUA LJ 12-6) while 2,2-dimethylpropane and 2,2,4-trimethylpentane were not simulated using the TAMie (AUA Mie 14-6) force field.

From Figures 4 and 5, we see that the Potoff S/L and TAMie force fields are not as accurate for these branched alkanes as for the normal alkanes. In particular, Potoff and TAMie demonstrate the same temperature dependence observed for other force fields, where the deviations are largest at lower temperatures. However, Potoff still provides considerable improvement compared to the LJ 12-6 based models, i.e., TraPPE and AUA4. Note that the performance is similar for the Potoff "short" and "long" parameters in Figures 4 and 5, respectively.

The deviations for each force field are largest for 2-methylpropane and 2,2-dimethylpropane. Since these compounds are primarily composed of CH$_3$ UA sites, this poor performance is likely due to the assumption that the CH$_3$ non-bonded parameters are transferable from n-alkanes to branched alkanes. Improvement might be possible if the CH$_3$ parameters were different depending on the neighboring UA site type. However, we emphasize that REFPROP states that the viscosity correlation for 2,2-dimethylpropane is not of "reference quality."
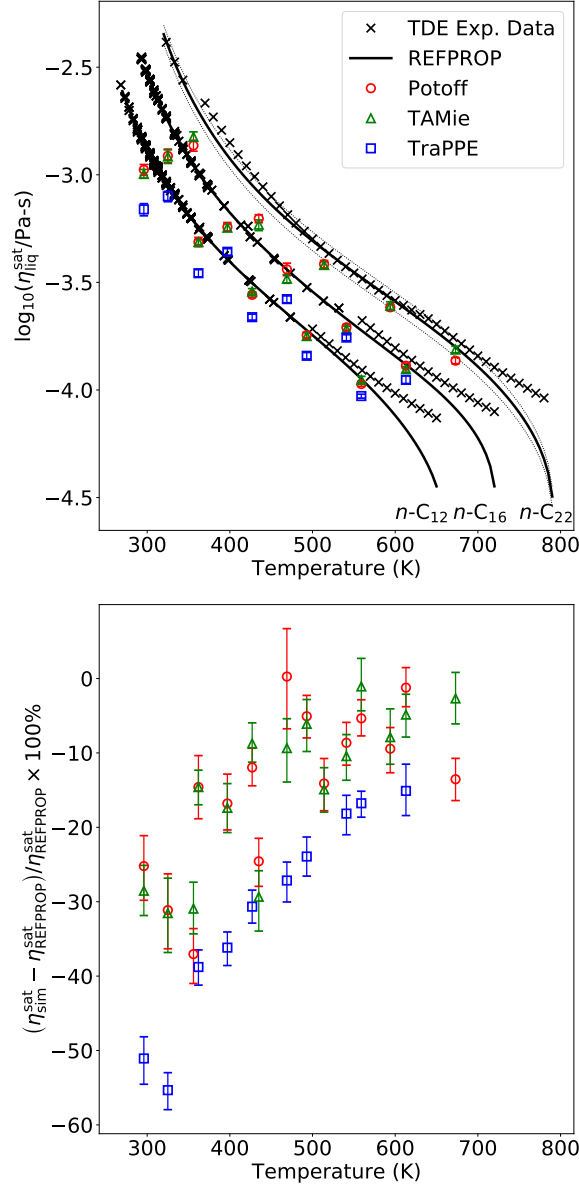
Figure 3: Saturated liquid viscosities for n-dodecane (n-C_{12}), n-hexadecane (n-C_{16}), and n-docosane (n-C_{22}). Top panel compares simulation results with REFPROP correlations and TDE data. Bottom panel computes the percent deviation between the simulation and REFPROP values. Colors/symbols denote different force fields.

3.2. Compressed liquid

Section 3.1 demonstrates that Mie n-6 based force fields (Potoff and TAMie) are considerably more reliable for predicting saturated liquid viscosities than LJ 12-6 based force
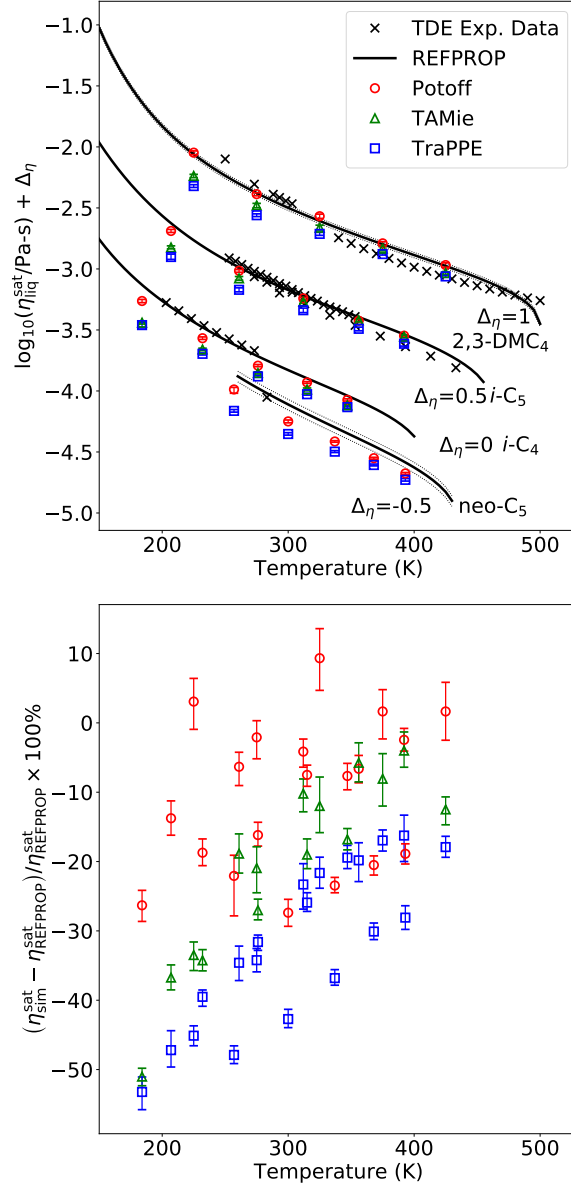
Figure 4: Saturated liquid viscosities for 2-methylpropane (i-C$_4$), 2,2-dimethylpropane (neo-C$_5$), 2-methylbutane (i-C$_5$), and 2,3-dimethylbutane (2,3-DMC$_4$). Top panel compares simulation results with REFPROP correlations and TDE data. Bottom panel computes the percent deviation between the simulation and REFPROP values. For clarity, values in top panel are shifted by Δ_η. Colors/symbols denote different force fields.

fields (TraPPE and AUA4). However, Reference 47 confirms that the Mie n-6 potential is too repulsive at short distances for $n > 12$, which causes the Potoff (16-6) and TAMie
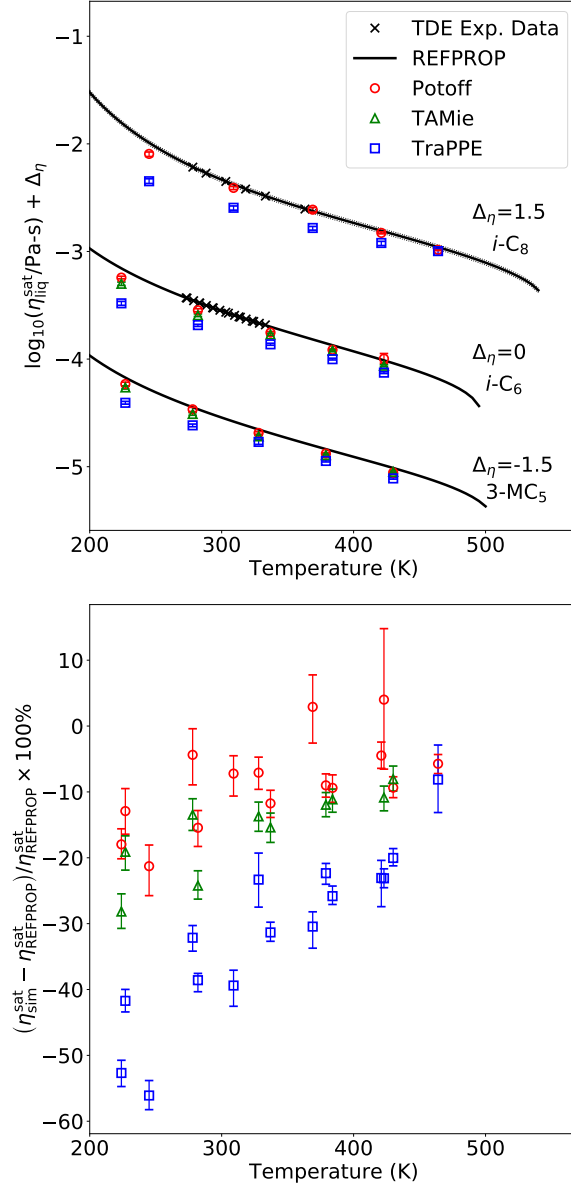
Figure 5: Saturated liquid viscosities for 2-methylpentane (i-C$_6$), 3-methylpentane (3-MC$_5$), and 2,2,4-trimethylpentane (i-C$_8$). Top panel compares simulation results with REFPROP correlations and TDE data. Bottom panel computes the percent deviation between the simulation and REFPROP values. For clarity, values in top panel are shifted by $\Delta\eta$. Colors/symbols denote different force fields.

(14-6) force fields to over estimate pressure at high densities. Since viscosity increases with a more repulsive potential (increasing n), our *ansatz* was that Potoff and TAMie would over

estimate η at high densities/pressures.

Surprisingly, Reference 12 shows that a (modified) Mie 14-6 (CH$_3$) and 20-6 (CH$_2$) potential can accurately predict the η-P dependence for n-hexadecane at 400 MPa. Note that Reference 12 did not report the η-ρ dependence, utilizes a slightly modified Mie formulation, and included saturated liquid viscosity data in the non-bonded parameterization. The purpose of this section is to determine if the Potoff 16-6 and TAMie 14-6 force fields are also reliable for estimating the η-P dependence. To provide additional insight into the consequences of using a Mie potential with $n > 12$, we present results for the η-ρ dependence as well.

3.2.1. Normal alkanes

Figures 6, 7, and 8 compare the elevated pressure viscosities for propane, n-butane, and n-octane, respectively. Each compound is simulated using the TraPPE, Potoff, and TAMie force fields at four or five densities. Simulation results are compared with REFPROP correlations and TDE data, when available. All TDE data for temperatures between 288 and 298 K are included. REFPROP uncertainties are assumed to be a constant percent deviation as reported in the corresponding publication. "REFPROP extrapolation" are values that lie outside of the "reference quality" range. This extrapolation is intended to guide the eye when comparing with simulation results at high densities/pressures.

Figure 6 demonstrates that the TraPPE force field has a constant negative bias even with increasing density/pressure. The TAMie force field has the most accurate η-ρ dependence, i.e., the error does not increase with respect to density. By contrast, the Potoff potential demonstrates considerable over estimation of η at high densities, which is likely attributed to the overly repulsive Mie 16-6 potential at close distances. Remarkably, the Potoff force field is the most accurate at predicting the η-P dependence from saturation pressure to 1 GPa. This can be explained as a cancellation of errors since the Potoff force field significantly over predicts both viscosity and pressure at high densities. Note that the increase in Potoff deviations for the two highest pressures can potentially be explained by the large uncertainty in the REFPROP correlation and extrapolation at these extreme pressures.
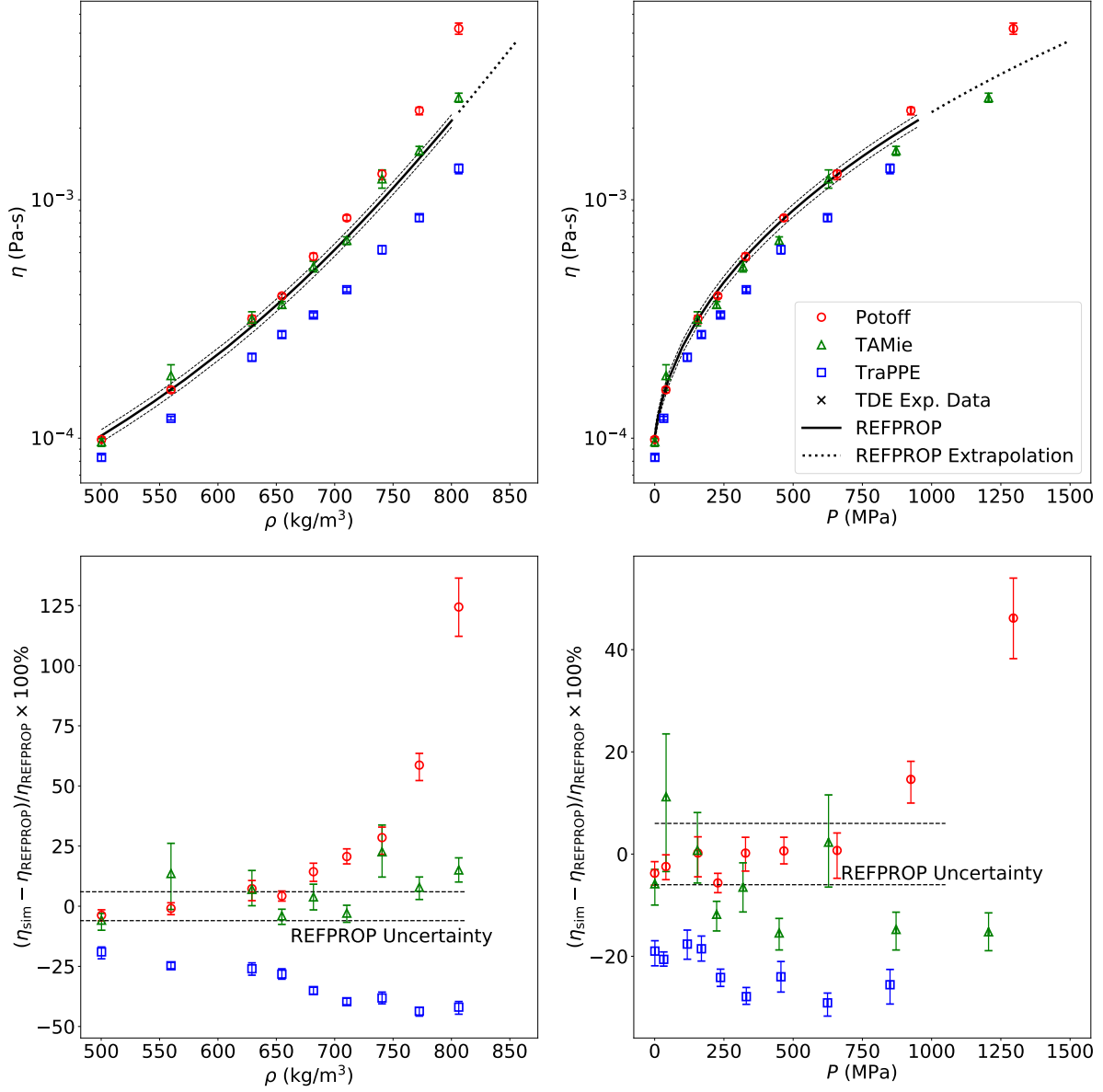
Figure 6: Compressed liquid viscosities at 293 K for propane. Top panels provide η-ρ and η-P dependence. Bottom panels present deviations between simulated (η_{sim}) and REFPROP (η_{REFPROP}) values with respect to ρ and P. Dashed lines correspond to REFPROP uncertainties. Dotted lines are extrapolation values outside of "reference quality" range. Colors/symbols denote different force fields and experimental data. Simulation uncertainties are obtained from bootstrap re-sampling and are presented at the 95 % confidence level.
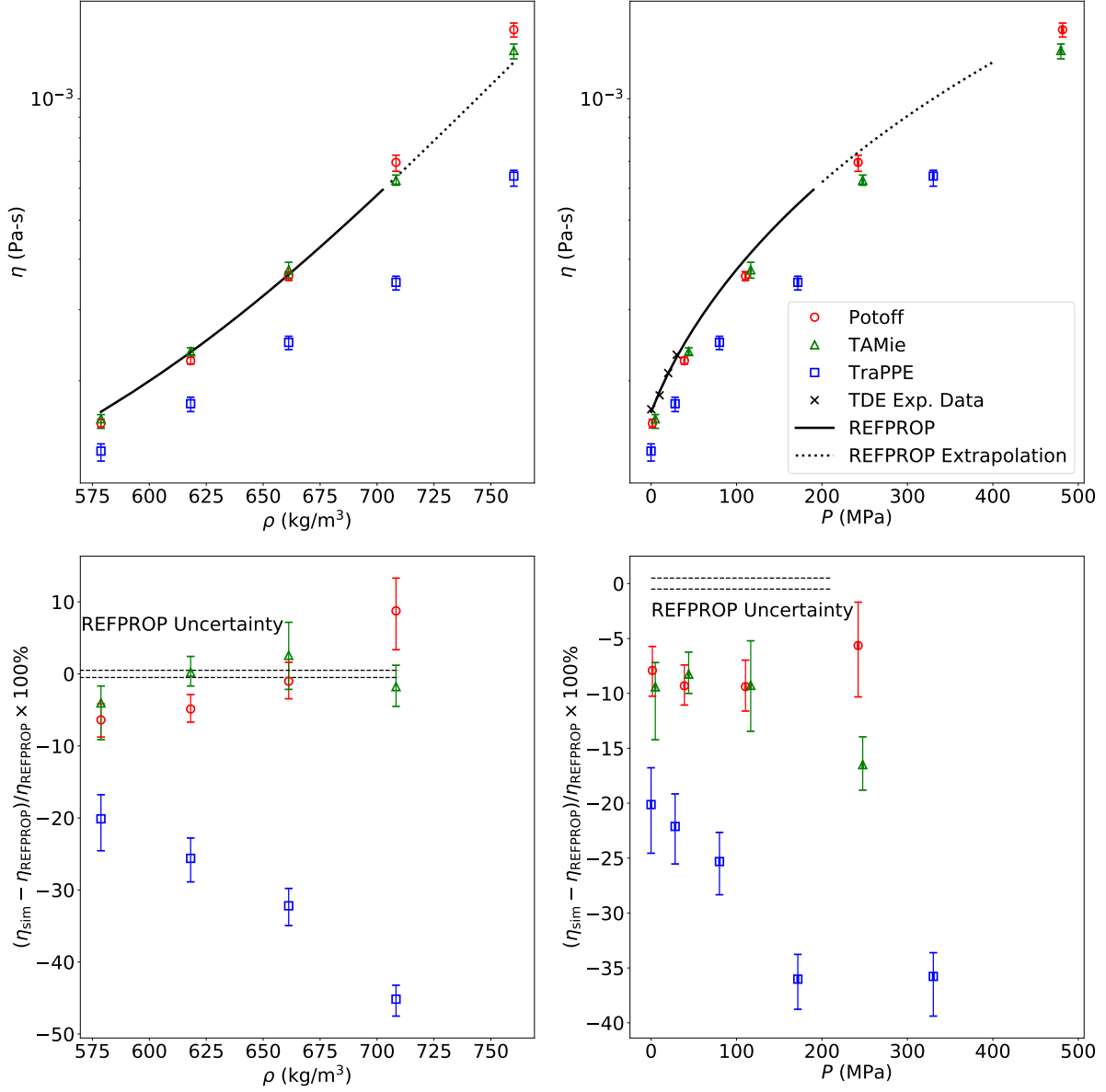
Figure 7: Compressed liquid viscosities at 293 K for n-butane. See caption of Figure 6.

The results in Figures 7 and 8 for n-butane and n-octane, respectively, are similar to those in Figure 6 for propane. Specifically, the TraPPE force field under predicts η at all densities/pressures, the TAMie force field provides the most accurate η-ρ dependence, while the Potoff force field over predicts η with respect to ρ but accurately predicts the η-P trend. We conclude that the Potoff force field is overly repulsive at short distances, and should not
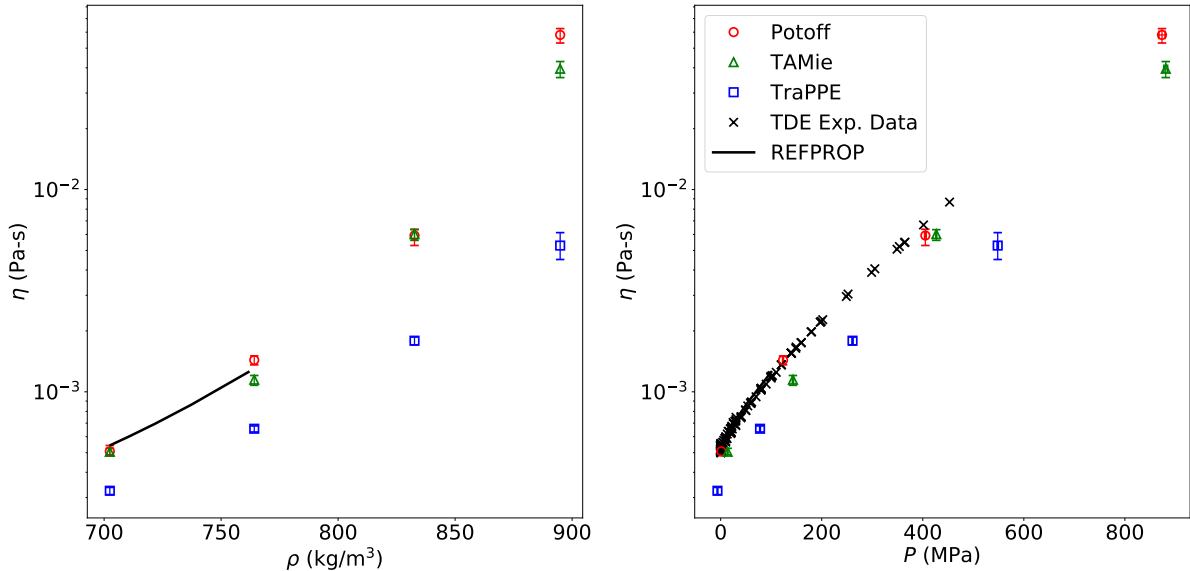
Figure 8: Compressed liquid viscosities at 293 K for *n*-octane. See caption of Figure 6.

be used to estimate the η-ρ dependence. However, the Potoff force field is the most reliable for estimating the η-P dependence, which is often the desired relationship in practice.

3.2.2. Branched alkanes

The trends observed in Figures 9 to 12 are consistent with the compressed liquid trends for *n*-alkanes. Specifically, TraPPE under-predicts the viscosity with respect to both ρ and P. Potoff over-predicts η with respect to ρ but provides a reasonable estimate of the η-P trend. As observed previously in Section 3.1, Potoff and TAMie are less accurate for branched alkanes than for *n*-alkanes. In particular, the Potoff η-P trends are systematically lower than the REFPROP correlations for 2-methylbutane and 3-methylpentane. However, note that the Potoff η-P trends are more reliable for 2-methylpropane and 2,2,4-trimethylpentane. These results cannot be attributed to the "short" or "long" parameter distinction.

4. Discussion/Limitations

While the Potoff force field significantly over-predicts the η-ρ dependence at $T = 293$ K, it does not over-predict η for the highest saturated liquid densities (those near the triple
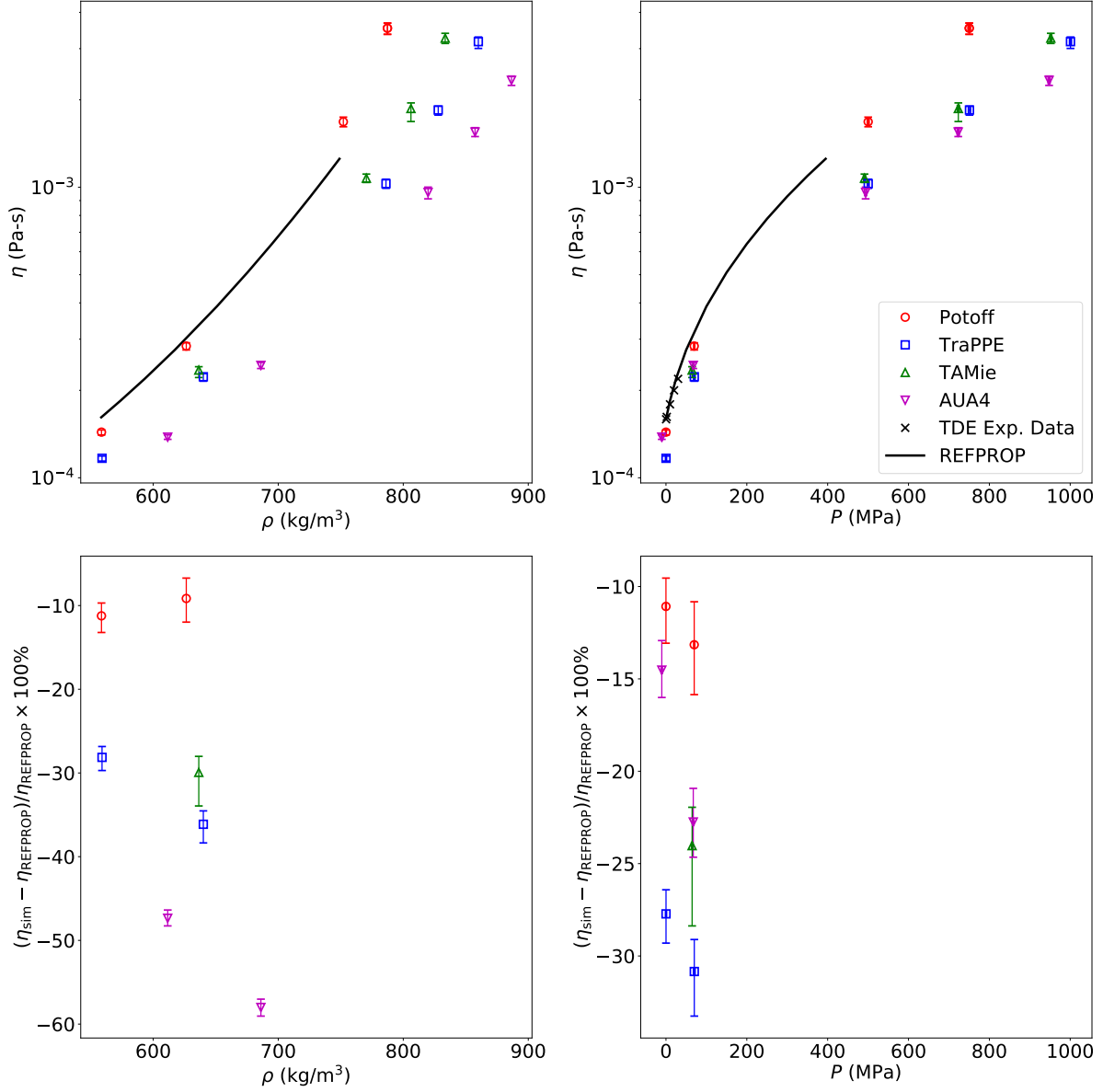
Figure 9: Compressed liquid viscosities at 293 K for 2-methylpropane. See caption of Figure 6.

point temperature) (cf. Figures 2 and 6). To better understand this, Figure 13 compares the radial distribution functions (RDF) for three different state points, namely, near the triple point ($T = 86$ K and $\rho = 732.63$ kg/m^3) and two densities along the $T = 293$ K isotherm ($\rho = 732.63$ kg/m^3 and $\rho = 806.23$ kg/m^3). Note that, in order to provide a fair comparison between force fields, the RDF is plotted with respect to a reduced distance, namely, $r/r_{\min}$.
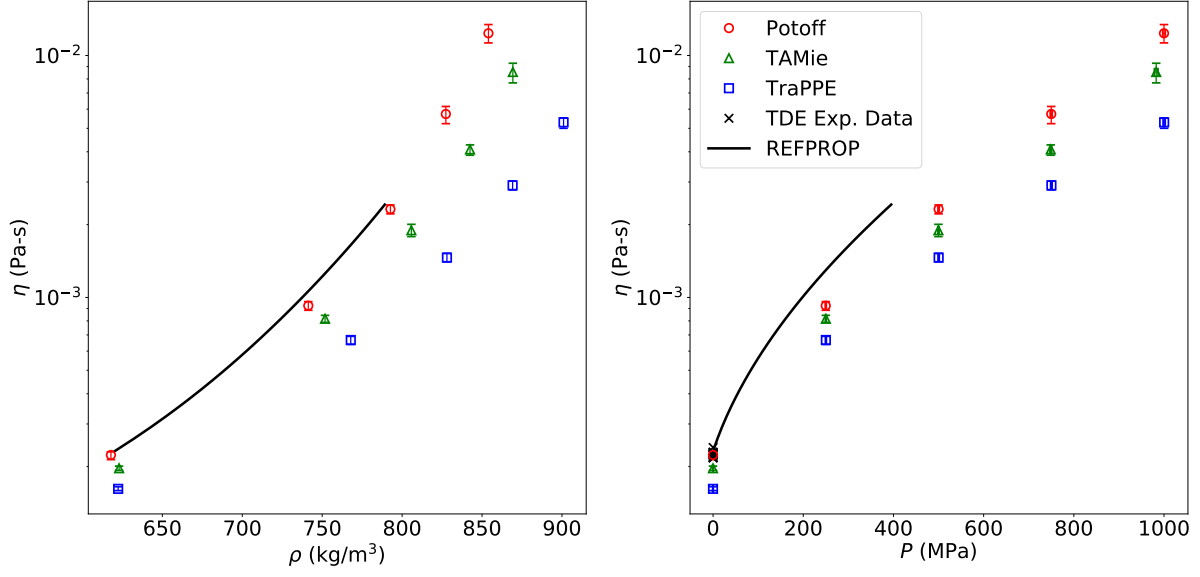
Figure 10: Compressed liquid viscosities at 293 K for 2-methylbutane. See caption of Figure 6.
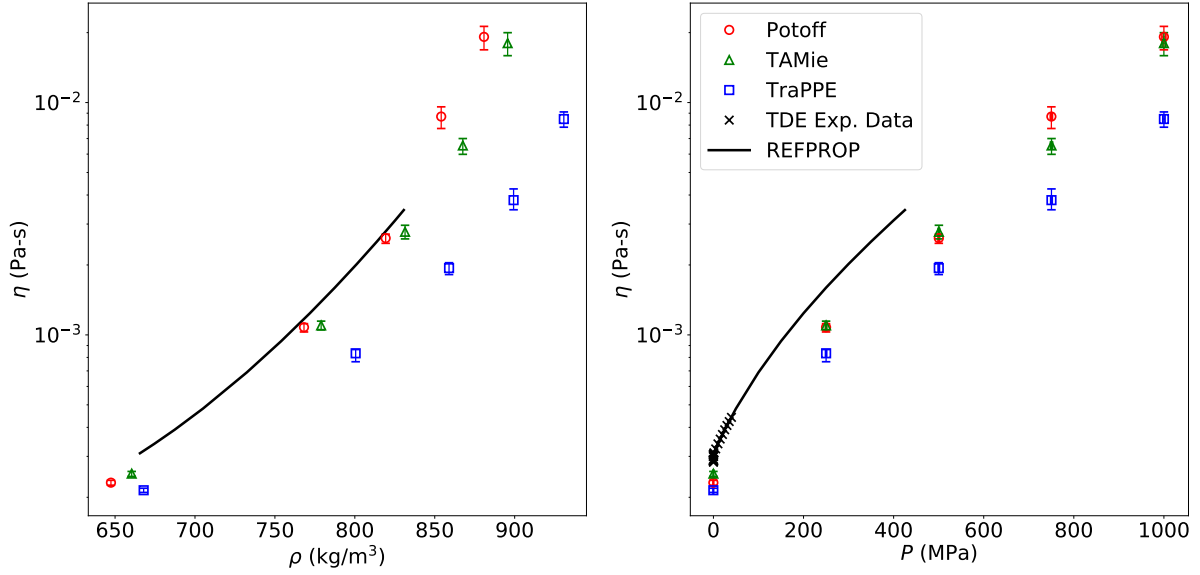

Figure 11: Compressed liquid viscosities at 293 K for 3-methylpentane. See caption of Figure 6.

The top panel of Figure 13 demonstrates that the RDF is shifted to the left (closer interactions) when increasing the temperature from 86 K to 293 K. Note that, although the magnitude of this shift is similar for all three force fields, the Potoff viscosities are impacted
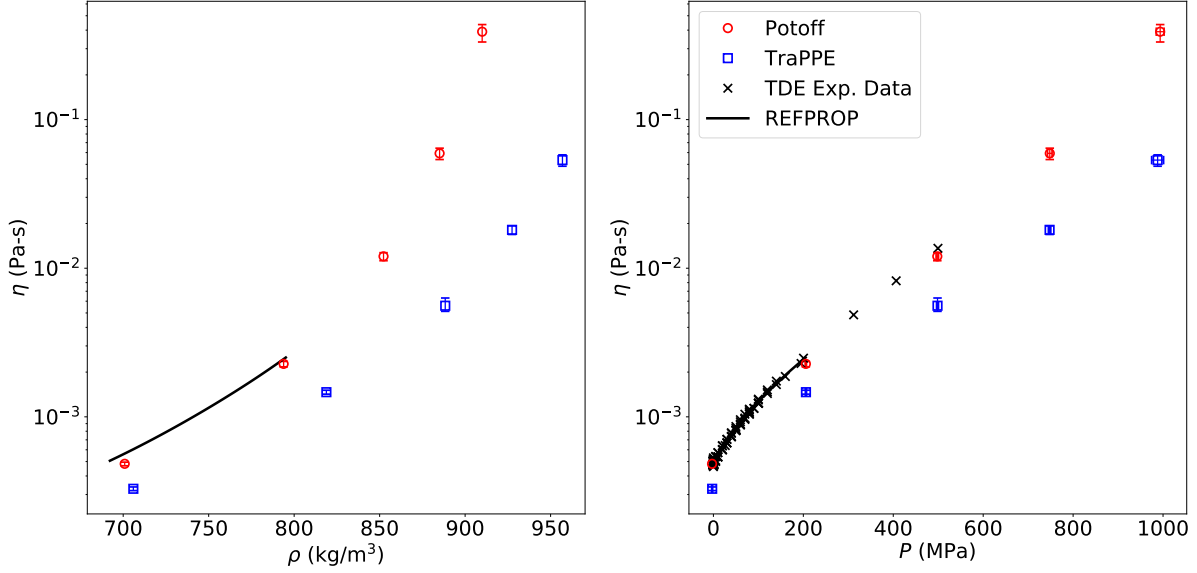
25

Figure 12: Compressed liquid viscosities at 293 K for 2,2,4-trimethylpentane. See caption of Figure 6.

the most from this shift due to the steepness of the Mie 16-6 potential. By contrast, the bottom panel demonstrates that increasing the density at constant temperature does not result in a shift but does increase the frequency of close-range interactions. Therefore, the overly repulsive Mie 16-6 potential is only problematic at high densities if there is sufficient thermal energy for the system to sample extremely close-range interactions. This explains why the Potoff force field is reliable at high densities along the saturation curve but over-estimates the η-ρ dependence at 293 K.

4.1. Finite-size effects

Previous studies have demonstrated that finite-size effects are often negligible for viscosity estimates with equilibrium molecular dynamics. However, since this analysis is typically not reported in the literature, the "Best Practices" guide recommends validating that finite-size effects are indeed negligible. For this reason, Figure 14 compares the results for simulations performed with 100, 200, 400, and 800 molecules of propane.

Notice that the averages and uncertainties typically overlap considerably and that there is no clear trend with respect to $N^{-1/3}$. In addition to this visual inspection, we also perform
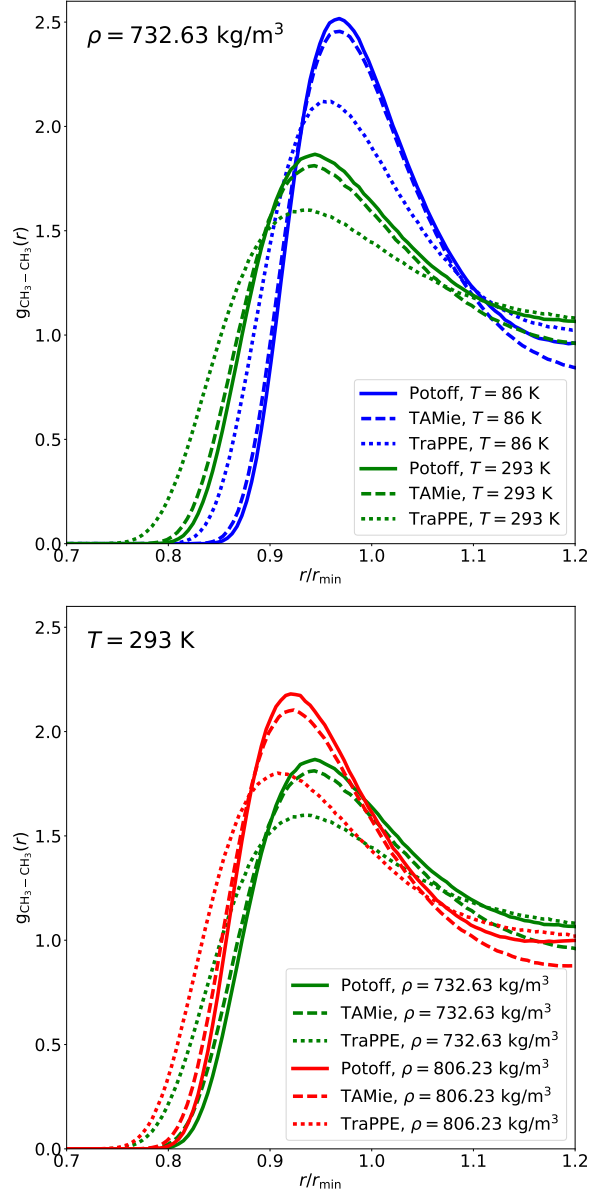
26

Figure 13: Comparison of radial distribution function ($g(r)$) for CH$_3$-CH$_3$ interactions. The top panel compares two different temperatures near the triple point isochore. The bottom panel compares two different densities along the 293 K isotherm. Colors correspond to different temperatures while line styles denote different force fields.

a "random permutation test" to determine that the results from the different system sizes are statistically indistinguishable. The algorithm for "random permutation testing" is the following:

Figure 14: Finite-size effects. Five different

1. Compute the "observed" sum-of-squares between the four different system sizes (SS_{obs})

2. Randomly divide the replicate simulations of each system size into four groups, "A", "B", "C", and "D"

3. Average the replicate Green-Kubo integrals of each group

4. Fit Equation 8 to the averages from Step 3

5. Calculate the "permutated" sum-of-squares between the four different groups (SS_{perm}

6. Repeat Steps 2 to 5 hundreds of times (N_{perm})

7. Count the number of permutations with $SS_{\text{perm}} > SS_{\text{obs}}$ (N_{count})

8. Assign a p-value equal to the ratio of N_{count} divided by N_{perm}

9. If $p > 0.05$, we fail to reject the Null-hypothesis that all four system sizes are statistically equivalent

This approach is employed in place of the standard Analysis of Variance (ANOVA) test because it is not possible to compute a reliable F-statistic. Computing an F-statistic requires computing the sum-of-squares between replicates, but an individual replicate simulation does not provide a meaningful estimate of η. Therefore, we can only compute the sum-of-squares between averages and not the sum-of-squares between replicates. However, since the sum-of-squares between replicates is a constant value regardless of the permutations, comparing

the sum-of-squares is equivalent to comparing the F-statistic.

4.2. Cut-off distance

The choice of cut-off distance is a subtle but important decision. In this study, we implement a 1.4 nm cut-off for each force field except Potoff, which utilizes only a 1.0 nm cut-off. This choice was made because the Potoff force field was parameterized with a 1.0 nm cut-off.

The "Best Practices" guide suggests that cut-off lengths could be significant but does not provide any convincing evidence to prove or disprove this notion. To address this issue, we perform simulations of the Potoff force field using three different cut-off distances. Specifically, Figure 15 presents the Potoff viscosity values for propane, n-butane, n-octane, and n-dodecane using cut-offs of 1.0 nm, 1.4 nm, 1.8 nm.

Figure 15: Impact of cut-off distance.

Figure 15 demonstrates that for smaller compounds the impact of cut-off is negligible, while a 1.0 nm cut-off causes a significant error for n-dodecane. For this reason, the Potoff results presented previously in Figure ?? were obtained using a 1.4 nm cut-off. In fact, n-hexadecane and n-docosane were unstable with a 1.0 nm cut-off and a 2 fs time-step. Reducing the time step to 1 fs was capable of stabilizing the 1.0 nm cut-off.

The instability of a 1.0 nm cut-off (with 2 fs time-steps) demonstrates the importance of verifying that the cut-off distance is long enough to not impact the system dynamics. Furthermore, this demonstrates why alternative tail modifications are ideal for molecular dynamics, e.g., force-shift and switch-force. Unfortunately, these tail modifications significantly impact saturation properties, suggesting that the non-bonded parameters must be re-optimized with the modified tail. Therefore, performing simulations with a force-shift or switch-force Potoff, TraPPE, TAMie, and AUA4 potential would likely result in inaccurate viscosities. Re-parameterizing the non-bonded interactions for a force-shift or switch-force potential is beyond the scope of this study.

4.3. $\rho_{\mathrm{liq}}^{\mathrm{sat}}$

There are at least three reasons why we perform simulations at the REFPROP $\rho_{\mathrm{liq}}^{\mathrm{sat}}$ instead of the force field $\rho_{\mathrm{liq}}^{\mathrm{sat}}$. First, this approach allows for a fair comparison of the force fields' ability to predict viscosity, without penalizing force fields which are less accurate at predicting $\rho_{\mathrm{liq}}^{\mathrm{sat}}$ or rewarding force fields that mask their deficiencies in predicting viscosity by over- or under-estimating $\rho_{\mathrm{liq}}^{\mathrm{sat}}$. Second, since each of the studied force fields utilized $\rho_{\mathrm{liq}}^{\mathrm{sat}}$ data in their optimization, deviations between the REFPROP and force field values are small, typically less than 1 %. However, small differences in density have been reported to result in large differences in viscosity. For this reason, a small set of validation simulations are performed to determine the variability caused by utilizing the REFPROP densities. The force field saturated liquid densities were obtained from the literature.

The use of REFPROP $\rho_{\mathrm{liq}}^{\mathrm{sat}}$ caused some simulations to be in a meta-stable state. Specifically, this occurs when the force field vapor pressure is less than the REFPROP vapor pressure. Fortunately, this is uncommon as Potoff, TAMie, and AUA4 are quite reliable for estimating $P_{\mathrm{vap}}^{\mathrm{sat}}$ and TraPPE significantly over-estimates $P_{\mathrm{vap}}^{\mathrm{sat}}$.

5. Conclusions

This study demonstrates the improvement that has taken place over the past two decades for predicting viscosity with molecular simulation. First, the "Best Practices" for EMD lead

to more reproducible results. Second, the state-of-the-art Mie n-6 force fields are significantly more accurate than the traditional Lennard-Jones 12-6 force fields. More specifically, the Potoff and TAMie force fields typically predict saturated liquid viscosities for n-alkanes to within 10 % of the REFPROP values. By contrast, the TraPPE and AUA4 models under-predict saturated liquid viscosities by 30 % to 50 %, where the deviations are largest at lower temperatures. While Potoff and TAMie are also more reliable for branched alkanes, deviations are larger and demonstrate a similar temperature dependence. The key limitation of the Potoff force field is that the choice of n= 16 is too repulsive at high densities, which causes the viscosity to be over-estimated at high densities. Due to a fortuitous cancellation of errors, the Potoff potential does provide a reliable η-P trend. Since TAMie uses n= 14, the η-ρ trend is slightly more reliable than that of Potoff. It is important to emphasize that transport properties were not included in the training set for parameterizing the Potoff and TAMie force fields. Therefore, the results from this study demonstrate that the improved prediction of static vapor-liquid coexistence properties obtained with Mie n-6 potentials also results in improved prediction of a transport property, namely, liquid viscosity.

[1] B.E. Poling, J.M. Prausnitz, and J.P. O'Connell. *The Properties of Gases and Liquids*. McGraw-Hill Companies, Inc., 2001. Chapter 9.

[2] Ángel Mulero, Isidro Cachadiña, and José O. Valderrama. Artificial neural network for the correlation and prediction of surface tension of refrigerants. *Fluid Phase Equilibria*, 451:60 − 67, 2017.

[3] Seongmin Lee, Kiho Park, Yunkyung Kwon, Tae-Yun Park, and Dae Ryook Yang. A modified scaled variable reduced coordinate (svrc)-quantitative structure property relationship (qspr) model for predicting liquid viscosity of pure organic compounds. *Korean Journal of Chemical Engineering*, 34(10):2715–2724, Oct 2017.

[4] Oliver L otgering-Lin and Joachim Gross. Group contribution method for viscosities based on entropy scaling using the perturbed-chain polar statistical associating fluid theory. *Industrial & Engineering Chemistry Research*, 54(32):7942–7952, 2015.

[5] Carlos Nieto-Draghi, Philippe Ungerer, and Bernard Rousseau. Optimization of the anisotropic united atoms intermolecular potential for n-alkanes: Improvement of transport properties. *The Journal of Chemical Physics*, 125(4):044517, 2006.

[6] Damien A. Bernard-Brunel and Jeffrey J. Potoff. Effect of torsional potential on the predicted phase behavior of n-alkanes. *Fluid Phase Equilibria*, 279(2):100 – 104, 2009.

[7] Edward J. Maginn, Richard A. Messerly, Daniel J. Carlson, Daniel R. Roe, and J. Richard Elliott. Best practices for computing transport properties 1. self-diffusivity and viscosity from equilibrium molecular dynamics v1. *Living Journal of Computational Molecular Science*, Pending publication, 2018.

[8] William Allen and Richard L. Rowley. Predicting the viscosity of alkanes using nonequilibrium molecular dynamics: Evaluation of intermolecular potential models. *The Journal of Chemical Physics*, 106(24):10273–10281, 1997.

[9] Rajdeep Singh Payal, S. Balasubramanian, Indranil Rudra, Kunj Tandon, Ingo Mahlke, David Doyle, and Roger Cracknell. Shear viscosity of linear alkanes through molecular simulations: quantitative tests for n-decane and n-hexadecane. *Molecular Simulation*, 38(14-15):1234–1241, 2012.

[10] Maurizio Mondello and Gary S. Grest. Viscosity calculations of n-alkanes by equilibrium molecular dynamics. *The Journal of Chemical Physics*, 106(22):9327–9336, 1997.

[11] Molecular simulation of the thermophysical properties of fluids: From understanding toward quantitative predictions. *Journal of Molecular Liquids*, 134(1):71 – 89, 2007. EMLG/JMLG 2005 Special Issue.

[12] Peter A. Gordon. Development of intermolecular potentials for predicting transport properties of hydrocarbons. *The Journal of Chemical Physics*, 125(1):014504, 2006.

[13] Hai Hoang, StÃĺphanie Delage-Santacreu, and Guillaume Galliero. Simultaneous description of equilibrium, interfacial, and transport properties of fluids using a mie chain coarse-grained force field. *Industrial & Engineering Chemistry Research*, 56(32):9213–9226, 2017.

[14] Carmelo Herdes, Tim S. Totton, and Erich A. Müller. Coarse grained force field for the molecular simulation of natural gases and condensates. *Fluid Phase Equilibria*, 406:91 – 100, 2015.

[15] M. G. Martin and J. I. Siepmann. Transferable potentials for phase equilibria. 1. United-atom description of n-alkanes. *The Journal of Physical Chemistry B*, 102(14):2569–2577, 1998.

[16] Marcus G. Martin and J. Ilja Siepmann. Novel configurational-bias monte carlo method for branched molecules. Transferable Potentials for Phase Equilibria. 2. United-Atom Description of Branched Alkanes. *The Journal of Physical Chemistry B*, 103(21):4508–4517, 1999.

[17] Mansi S. Shah, J. Ilja Siepmann, and Michael Tsapatsis. Transferable potentials for phase equilibria. Improved united-atom description of ethane and ethylene. *AIChE Journal*, 63(11):5098–5110, 2017.

[18] J. J. Potoff and D. A. Bernard-Brunel. Mie potentials for phase equilibria calculations: Applications to alkanes and perfluoroalkanes. *The Journal of Physical Chemistry B*, 113(44):14725–14731, 2009.

[19] Jason R. Mick, Mohammad Soroush Barhaghi, Brock Jackman, Loren Schwiebert, and Jeffrey J. Potoff. Optimized mie potentials for phase equilibria: Application to branched alkanes. *Journal of Chemical & Engineering Data*, 62(6):1806–1818, 2017.

[20] Philippe Ungerer, Christele Beauvais, Jerome Delhommelle, Anne Boutin, Bernard Rousseau, and Alain H. Fuchs. Optimization of the anisotropic united atoms intermolecular potential for n-alkanes. *The Journal of Chemical Physics*, 112(12):5499–5510, 2000.

[21] Carlos Nieto-Draghi, Anthony Bocahut, Benoît Creton, Pascal Have, Aziz Ghoufi, Aurélie Wender, , Anne Boutin, Bernard Rousseau, and Laurent Normand. Optimisation of the dynamical behaviour of the anisotropic united atom model of branched alkanes: application to the molecular simulation of fuel gasoline. *Molecular Simulation*, 34(2):211–230, 2008.

[22] Andrea Hemmen and Joachim Gross. Transferable anisotropic united-atom force field based on the Mie potential for phase equilibrium calculations: n-alkanes and n-olefins. *The Journal of Physical Chemistry B*, 119(35):11695–11707, 2015.

[23] Dominik Weidler and Joachim Gross. Transferable anisotropic united-atom force field based on the mie potential for phase equilibria: Aldehydes, ketones, and small cyclic alkanes. *Industrial & Engineering Chemistry Research*, 55(46):12123–12132, 2016.

[24] M. P. Allen and D. J. Tildesley. *Computer Simulation of Liquids*. Clarendon Press ; Oxford University Press, Oxford England New York, 1987.

[25] M.J. Abraham, D. van der Spoel, E. Lindahl, B.Hess, and the GROMACS development team. *GROMACS User Manual version 2018, www.gromacs.org (2018)*, 2018.

[26] GROMACS non-bonded tail corrections assume that the long-range contribution from the $r^{-\lambda}$ term is negligible compared to the r^{-6} term. By comparing the GROMACS output with other (slower) simulation packages, we verified that the small error introduced with this approximation does not significantly affect our results. For this reason,

although it is straightforward to include the $r^{-\lambda}$ contribution, we did not attempt to modify the GROMACS default tail correction values.

[27] Yong Zhang, Akihito Otani, and Edward J. Maginn. Reliable viscosity calculation from equilibrium molecular dynamics simulations: A time decomposition method. *Journal of Chemical Theory and Computation*, 11(8):3537–3546, 2015.

[28] E. W. Lemmon, M. L. Huber, and M. O. McLinden. NIST Standard Reference Database 23: Reference Fluid Thermodynamic and Transport Properties-REFPROP, Version 9.1, National Institute of Standards and Technology, 2013.

[29] D. Bücker and W. Wagner. A reference equation of state for the thermodynamic properties of ethane for temperatures from the melting line to 675 K and pressures up to 900 MPa. *Journal of Physical and Chemical Reference Data*, 35(1):205–266, 2006.

[30] Eckhard Vogel, Roland Span, and Sebastian Herrmann. Reference correlation for the viscosity of ethane. *Journal of Physical and Chemical Reference Data*, 44(4):043101, 2015.

[31] Eric W. Lemmon, Mark O. McLinden, and Wolfgang Wagner. Thermodynamic properties of propane. iii. a reference equation of state for temperatures from the melting line to 650 K and pressures up to 1000 MPa. *Journal of Chemical & Engineering Data*, 54(12):3141–3180, 2009.

[32] Eckhard Vogel and Sebastian Herrmann. New formulation for the viscosity of propane. *Journal of Physical and Chemical Reference Data*, 45(4):043103, 2016.

[33] D. Bücker and W. Wagner. Reference equations of state for the thermodynamic properties of fluid phase n-butane and isobutane. *Journal of Physical and Chemical Reference Data*, 35(2):929–1019, 2006.

[34] Sebastian Herrmann and Eckhard Vogel. New formulation for the viscosity of n-butane. *Journal of Physical and Chemical Reference Data*, 47(1):013104, 2018.

[35] R. Beckmueller, M. Thol, and R. Span. Fundamental equation of state for n-octane. *International Journal of Thermophysics*, Pending publication, 2018.

[36] Marcia L. Huber, Arno Laesecke, and Hong Wei Xiang. Viscosity correlations for minor constituent fluids in natural gas: n-octane, n-nonane and n-decane. *Fluid Phase Equilibria*, 224(2):263 – 270, 2004.

[37] Eric W. Lemmon and Marcia L. Huber. Thermodynamic properties of n-dodecane. *Energy & Fuels*, 18(4):960–967, 2004.

[38] Marcia L. Huber, Arno Laesecke, and Richard Perkins. Transport properties of n-dodecane. *Energy & Fuels*, 18(4):968–975, 2004.

[39] R. Romeo and E.W. Lemmon. To be submitted. 2018.

[40] Private communication to M. Huber from V. Vesovic, Oct. 2017.

[41] M.L. Huber. Models for the viscosity, thermal conductivity, and surface tension of selected pure fluids as implemented in refprop v10.0. *NISTIR 8209*, Pending publication, 2018.

[42] Eric W. Lemmon and Roland Span. Short fundamental equations of state for 20 industrial fluids. *Journal of Chemical & Engineering Data*, 51(3):785–850, 2006.

[43] E. Vogel, C. Küchenmeister, and E. Bich. Viscosity correlation for isobutane over wide ranges of the fluid region1. *International Journal of Thermophysics*, 21(2):343–356, Mar 2000.

[44] K. Gao, J. Wu, and E.W. Lemmon. Unpublished equation. 2017.

[45] T.M. Blackham, A.K. Lemmon, and E.W. Lemmon. Fundamental equation of state for isooctane. *International Journal of Thermophysics*, Pending publication, 2018.

[46] Michael Frenkel, Robert D. Chirico, Vladimir Diky, Xinjian Yan, Qian Dong, and Chris Muzny. Thermodata engine (TDE): software implementation of the dynamic data evaluation concept. *Journal of Chemical Information and Modeling*, 45(4):816–838, 2005.

[47] Richard A. Messerly, Michael R. Shirts, and Andrei F. Kazakov. Uncertainty quantification confirms unreliable extrapolation toward high pressures for united-atom mie λ-6 force field. *Journal of Chemical Physics*, Pending publication, 2018.

6. Supporting Information

6.1. Gromacs input files

We have provided example input files for simulating *n*-isooctane at BLANK K with the Potoff force field in GROMACS (see attached .gro, .top, and .mdp files). Additionally, all files that were used to generate the results from this study can be found that the GitHub repository www.github.com/ramess101/IFPSC_10.

6.2. Tabulated values

1. Ethane
    (a) Saturation
        i. Potoff
        ii. TraPPE
        iii. AUA4
        iv. TAMie
    (b) T293 highP
        i. Potoff
        ii. TraPPE
        iii. AUA4
        iv. TAMie
2. Propane

    (a) Saturation

        i. Potoff

        ii. TraPPE

        iii. AUA4

        iv. TAMie

    (b) T293 highP

        i. Potoff

        ii. TraPPE

        iii. AUA4

        iv. TAMie

3. n-Butane

    (a) Saturation

        i. Potoff

        ii. TraPPE

        iii. AUA4

        iv. TAMie

    (b) T293 highP

        i. Potoff

        ii. TraPPE

        iii. AUA4

        iv. TAMie

Repeat for all other compounds with corresponding potentials

6.3. Simulation length effects

For less viscous systems, i.e., saturation and low pressures, a 1 ns simulation is typically sufficient for the Green-Kubo integral to reach a plateau. However, even when an apparent plateau is observed, too short of simulations can lead to systematic bias in η. For this reason, as recommended by "Best Practices," we verify that the estimated viscosity obtained from a 1 ns trajectory is consistent with that obtained from 2 ns, 4 ns, and 8 ns simulations.

Figure 16: Finite-size effects.

For more viscous systems, i.e., greater than 100 MPa, a 1 ns simulation is too short to observe a plateau in the Green-Kubo integral. In these cases, we increased the simulation time to a value between 2 and 8 ns. Due to the increased computational cost of such simulations, we did not perform an exhaustive test with increasing simulation time. Instead, the choice of simulation time was determined primarily by the ability to detect a plateau region. Therefore, it is possible that even longer simulations are required for the most viscous systems.

Due to inherently slow dynamics in highly viscous systems (greater than 0.02 Pa-s), obtaining well-converged Green-Kubo integrals is extremely challenging. Additional replicate simulations can help reduce noise.

Storage limitations become a concern with simulations longer than 8 ns due to the frequency at which data are output (every 6 fs). Reading in these files for GROMACS to evaluate the data nearly crippled our computing cluster.

Obtaining well-converged Green-Kubo integrals for highly viscous systems (greater than 0.02 Pa-s) is challenging and requires longer simulations.

6.4. Validation Runs

To validate our methodology, we attempt to replicate viscosity estimates available on the NIST Reference Simulation Data website for TraPPE-UA ethane as well as literature values for TraPPE-UA n-octane. Figure 17 compares the ethane and n-octane results from this study with those from NIST and the literature, respectively.

Figure 17: Comparison with NIST Reference Simulation Data and Reference **?** .

The n-octane validation is somewhat more useful than the ethane validation for at least three reasons. First, n-octane includes angle and torsional contributions that are absent in ethane. Second, the literature provides values for both rigid and flexible bonds. Third, the n-octane results are for fixed elevated pressures, which provides validation of our NPT ensemble results.

6.5. Bond types, Harmonic vs LINCS

To test how sensitive the results presented in Section 3 are to the use of fixed bond-lengths, we perform additional simulations with flexible bonds. Specifically, we use the traditional harmonic bond potential:

$$u^{\text{bond}} = \frac{k_{\text{b}}}{2} \left(r - r_{\text{eq}} \right)^2 \tag{9}$$

where u^{bond} is the bonded potential, k_{b} is the harmonic force constant, and r_{eq} is the equilibrium bond-length. To determine the impact, we perform simulations with two different

values of k_b, namely, BLANK (taken from reference BLANK) and BLANK (an arbitrarily large value). Figure 18 demonstrates that the difference between fixed and flexible bonds is negligible in certain cases, but for the larger force constant a systematic increase in viscosity is observed. Bootstrap resampling confirms that the LINCS and k_b = BLANK results are statistically indistinguishable, while the k_b = BLANK is statistically different.

Figure 18: Fixed bond-lengths compared with two different harmonic bond potentials.

6.6. Green-Kubo analysis

This section provides a detailed example of how we obtain estimates for η with its corresponding uncertainty. Figure BLANK depicts a typical autocorrelation function obtained by executing the GROMACS "energy –vis." By default, GROMACS partitions the complete simulation into twelve evenly sized time blocks. Therefore, the autocorrelation in Figure BLANK is the average of twelve different time origins. GROMACS then performs a simple trapezoidal integration of neighboring points to obtain the Green-Kubo integral. The Green-Kubo integral with respect to time is output in the "visco.xvg" file. Figure BLANK presents the Green-Kubo integral from forty replicate simulations. Although a single replicate is often quite noisy at long times, the average of these replicates converges smoothly (see Figure BLANK). Figure BLANK shows that the fluctuations, or standard deviation, increases with time but is adequately modeled with At^b. The line labeled "cut-off" in Figures

41

BLANK and BLANK is the time at which $\sigma_\eta \approx \eta^\infty$. Data beyond this time are excluded from the fit of the double-exponential function. Bootstrap resampling provides an estimate of the uncertainty. Figure BLANK shows that, typically, the bootstrapped distribution is quite normal. The line labeled "bootstraps" in Figure BLANK are the lower and upper 95 % confidence interval.

The results depicted in Figure BLANK are from BLANK, BLANK, BLANK.

Figure 19: Autocorrelation function with respect to time.

Figure 20: Replicate simulations, average, fit to average, cut-off, and bootstrap uncertainties.

Figure 21: Standard deviation of replicate simulations with respect to time.

Figure 22: Bootstrap distribution of η.

6.7. MCMC?